MR Imaging of Acute Intracranial Hemorrhage: Findings on Sequential Spin-Echo and Gradient-Echo Images in a Dog Model

Karen Weingarten[1]
Robert D. Zimmerman
Vishnu Deo-Narine
John Markisz
Patrick T. Cahill
Michael D. F. Deck

Seven intraparenchymal hematomas (four venous and three arterial) were placed in the brains of six dogs in order to study the MR appearance of acute hemorrhage and to evaluate the effects of several variables on the signal intensity of the hematoma. MR imaging at 0.6 and 1.5 T was performed by using standard short and long TR spin-echo and low-flip-angle gradient-echo sequences. Sequential examinations were performed during the first week following hematoma creation. MR findings were compared with CT and postmortem examinations. Three patterns of signal intensity were observed, which varied according to the size (small vs large) and location (parenchymal vs intraventricular) of the hematomas. The small parenchymal hematomas did not undergo evolutionary changes. On short TR scans they were isointense at both field strengths, and therefore not detectable; on long TR scans these hematomas were of variable intensity at 1.5 T and were hyperintense at 0.6 T. On gradient-echo scans, they were hypointense at all times at both field strengths. The large parenchymal hematomas underwent evolutionary changes typical of those seen in clinical imaging. On short TR scans they were initially isointense and became hyperintense 1–3 days later. Long TR scans demonstrated initial hyperintensity, followed by the development of hypointensity within 12 hr in the venous hematomas and within 60 hr in the arterial hematoma. The intensity changes on long TR scans were seen at both 0.6 and 1.5 T, but occurred sooner and to a greater degree at 1.5 T. Gradient-echo imaging of these large lesions demonstrated hypointensity at all times at both field strengths. The intraventricular hemorrhages demonstrated more rapid development of hyperintensity on short TR scans and slower and less pronounced development of hypointensity on long TR scans compared with the parenchymal clots in the same animal. Gradient-echo imaging of the intraventricular hemorrhages demonstrated hypointensity at all times at both field strengths.

A multifactorial hypothesis is proposed to explain the differences in intensity between venous, arterial, and intraventricular blood. Gradient-echo sequences should prove to be highly useful in detecting and delineating hemorrhages and are recommended for the MR protocol of patients with acute neurologic ictus and suspected hemorrhage.

***AJNR* 12:457–467, May/June 1991**

Acute intracranial hemorrhage undergoes rapid and complex changes in intensity that have been extensively investigated in vitro and in vivo [1–9]. The MR signal intensity of hemorrhage is influenced by several intrinsic and extrinsic factors [6]. The intrinsic factors include the time from ictus and the source, size, and location of hemorrhage; the extrinsic factors include the pulse sequence and the field strength. In order to conduct a clinical study to assess the contribution of each of these parameters to the intensity of acute hematoma, it would be necessary to perform serial examinations on multiple patients on scanners of different field strengths within a few days after hemorrhage, a nearly impossible task. In the one comparative clinical evaluation of 50 patients with acute hemorrhage imaged at both 0.5 and 1.5 T [10], only seven were evaluated during the first week, none were evaluated within 24 hr, and no serial studies were performed. To improve our knowledge of the appearance of acute hemorrhage and to determine the effects

Received May 9, 1990; revision requested August 7, 1990; revision received November 27, 1990; accepted December 11, 1990.

Presented in part at the annual meetings of the American Society of Neuroradiology, New York City, May 1987, and Chicago, May 1988.

[1] All authors: Department of Radiology, The New York Hospital–Cornell Medical Center, 525 E. 68th St., New York, NY 10021. Address reprint requests to K. Weingarten.

0195–6108/1203–0457

TABLE 1: Summary of Experimentally Produced Hematomas and MR Imaging Times in Dogs

Dog No.	Blood Source	Amount Injected (ml)	Clot Size (cm)	Imaging Times
1	Venous	1.5	0.8 × 0.2 × 0.2 (S)	0, 9, 14, 24 hr
2	Venous	2.5	1.5 × 0.2 × 0.1 (S)	0, 8, 24, 36, 60 hr
3	Venous	5	1.5 × 1.1 × 0.4 (L)	0, 12, 24, 36 hr
4	Arterial	4.5	1.3 × 1.1 × 0.5 (L)	0, 16, 24, 60 hr
5[a]	Arterial	4	1.0 × 0.2 × 0.2 (S)	0, 48, 96 hr; 8 d
	Arterial	5	1.5 × 0.6 × 0.3 (S)	0, 24, 72 hr; 7 d
6	Venous	5	1.2 × 1.1 × 1.0 (L)	0, 12, 24, 72 hr; 8 d

Note.—Clot size was measured on the pathologic specimen. Zero-hour images were not obtained in dog 3 at 1.5 T. Parenchymal and intraventricular hemorrhage were present in dogs 2 and 6. S = small; L = large.

[a] Hematomas were injected bilaterally in dog 5.

of various parameters on hematoma signal intensity, an in vivo animal model was used. Seven hematomas were created by injecting arterial or venous blood into the brains of six dogs (one dog received two injections), and sequential imaging was performed on 0.6- and 1.5-T clinical MR imagers using spin-echo (SE) and gradient-echo (GE) sequences. The implications of our findings with respect to both routine clinical imaging and current hypotheses on the mechanisms underlying hematoma intensity are discussed.

Materials and Methods

Six dogs (three male, three female), each weighing 10–12 kg, were used. Seven hematomas were created, with five animals receiving a unilateral hematoma in the frontoparietal region. Hematomas were injected bilaterally in one dog because of the very small size of the initial hematoma and the clinical stability of the animal. The dogs were placed in an MR-compatible Lucite head holder that was attached to a stereotaxic frame. Under endotracheal anesthesia and with aseptic technique, a burr hole was surgically created with a standard dental drill, with care taken to avoid penetrating the dura. After the burr hole was cleaned, 1.5–5 ml of blood was removed from a peripheral artery or vein of the animal and, under stereotaxic control, immediately injected through the burr hole with an 18-gauge spinal needle to a depth of 1 cm from the inner table of the calvaria. The needle was then removed and the burr hole was covered with bone wax. A small aliquot of the sample was not injected so as to be used for immediate blood gas analysis. Thus, by using autologous blood, seven parenchymal hematomas were created with the use of venous blood in dogs 1–3 and 6 and arterial blood in dogs 4 and 5.

MR imaging of each hematoma was performed at both 0.6 T (Technicare) and 1.5 T (General Electric) immediately after generation of each hematoma, at several times during the first 48 hr, and at various times during the subsequent 6 days. The time interval between sequential imaging of the same lesion and the total number of scans obtained in each animal were dependent on the dual availability of the MR imagers and the medical condition of the animals (Table 1). For logistical reasons, at each imaging time, scans were always obtained initially at 0.6 T and then immediately thereafter at 1.5 T. The average time between the onset of scanning at 0.6 and 1.5 T was 1 hr; the maximum elapsed time was 2 hr, which occurred in one dog 72 hr after hematoma production. A variety of pulse sequences were used; these are listed, along with pertinent technical information, in Table 2. In brief, comparable short TR/short TE and long TR/multiecho SE sequences were acquired at both field strengths. The long TR scans were done with a short TE (<30 msec), an intermediate TE (30–60 msec), and a long TE (>60 msec). A variety of GE sequences were obtained. Because of technical constraints, the TR, TE, and flip angles were not comparable on the two imagers, though, in general, all GE sequences were relatively T2-weighted. The size, location, and configuration of each hematoma were evaluated. Two neuroradiologists jointly compared the intensity of each lesion relative to internal references, in particular, normal brain on short TR scans and normal gray matter on long TR and GE scans. The predominant intensity of each hematoma on the short TR, long TR, and GE sequences was assigned a numerical value of −2, −1, 0, +1, or +2, which indicated moderate hypointensity, mild hypointensity, isointensity, mild hyperintensity, or moderate hyperintensity, respectively, compared with the reference tissue of each pulse sequence. No attempt was made to measure T1 or T2 values directly since the small size and complex shape of these lesions precluded accurate quantitative determinations.

TABLE 2: MR Parameters Used when Imaging Dogs with Experimentally Produced Hematomas

Variable	0.6 T	1.5 T
Slice thickness (mm)	7.5	5.0
Interslice gap (mm)	2.5	2.5
Acquisition matrix	128 × 256	256 × 256
No. of excitations	2	2
Spin-echo sequences		
Short TR/short TE	500/30	500/30
Long TR/long TE	2000/100	2000/100
Long TR/multiecho TE	2000/25, 50, 75, 100[a]	2000/25, 50, 75, 100[a]
	2000/50, 100[b]	2000/50, 100[b]
Gradient-echo sequences (TR/TE/flip angle)	500/30/30°	25–75/10–17/10°
	500/60/30°	
	1000/60/30°	
Technique	Multislice	Single slice

Note.—Gradient-echo images were not obtained in dogs 1 and 2 at 0.6 T.

[a] Dogs 1–3 only.

[b] Dogs 4–6 only.

An unenhanced CT scan (General Electric 8800 or 9800 unit) was acquired during the first 6 hr after injection of each hematoma by using contiguous 5-mm sections with the dog in the Lucite head holder. The ability of MR and CT to detect, delineate, and characterize hemorrhage was compared. Furthermore, the CT scans were used to assess for the presence of injection-created artifacts that might affect hematoma intensity.

The animals were sacrificed at the termination of each experiment. The brains were fixed in formalin and sectioned in the coronal plane, and the MR findings were correlated with gross pathology. The size of each hematoma was measured from the pathologic specimen after correction for shrinkage of the brain due to formalin fixation. (The correction factor for each brain was calculated by measuring its length and width before and after fixation.) Our experimental protocol conformed to the National Institutes of Health guidelines for animal research.

One clinical case, a patient with an acute right frontal convexity subdural hematoma, was included in this study. This patient was imaged 60 hr after hemorrhage with SE 600/20 and 2000/40,80 sequences at both 0.6 and 1.5 T.

Results

There was a clear-cut difference in the intensity of hemorrhage on serial studies according to the size and location of the hematoma. The lesions were divided into three subgroups: (1) small (<1 cm in at least two dimensions on gross pathology), (2) large (>1 cm in at least two dimensions on gross pathology), and (3) intraventricular. Time/intensity bar graphs of the intensity of each of the subgroups on short TR/TE, long TR/TE, and GE sequences were plotted relative to reference tissues. For those time frames in which more than one hematoma in the subgroup was imaged, the average intensity was plotted.

The appearance of the four small hematomas in dogs 1, 2, and 5 (two hematomas) was not affected by the source of hemorrhage, nor did the hematomas undergo the changes in intensity characteristic of hemorrhage in clinical practice (Figs. 1 and 2). These lesions were isointense and hence not detectable on short TR/TE scans at either field strength (Fig. 2C). On long TR/long TE scans at 1.5 T, they were of variable intensity, demonstrating central hyper-, iso-, or hypointensity and peripheral hyperintensity (Figs. 1, 2D, and 2G). At 0.6 T these hematomas were homogeneously and persistently hyperintense (Figs. 1 and 2E). On GE scans all of the small hematomas were readily detectable as nodular foci of hypointensity regardless of the time from ictus, the source of hemorrhage, or the field strength of the MR imager (Figs. 2H and 2I).

The three "large" hematomas in dogs 3, 4, and 6, despite being small by clinical standards, underwent evolutionary changes similar to those observed in clinical practice (Figs. 3–6). On short TR/TE scans these hematomas were initially isointense (Fig. 4C) and subsequently became hyperintense. The temporal changes in intensity on short TR/TE sequences were independent of the field strength but dependent on the source of hemorrhage (Figs. 3A and 3B). Specifically, the venous hematomas demonstrated initial hyperintensity by 72 hr and maximal hyperintensity by 8 days, whereas the arterial hematomas developed hyperintensity earlier (16 hr) and achieved maximal hyperintensity quicker (60 hr) (compare Figs. 4D and 6C, 4E and 6D).

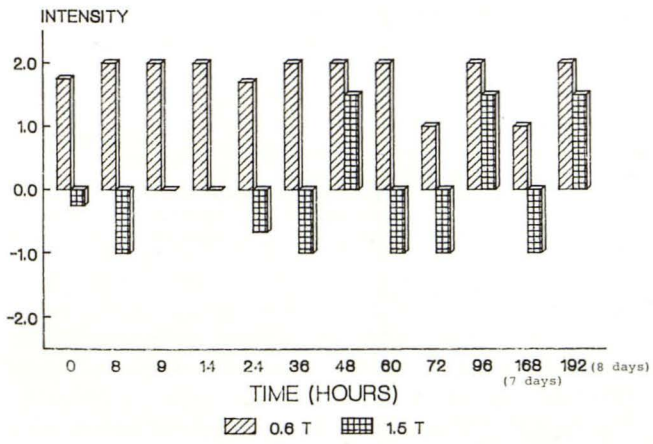

Fig. 1.—Time/intensity bar graph for small hematomas on long TR scans. Note variable intensity at 1.5 T and persistent hyperintensity at 0.6 T.

On long TR/TE scans the large hematomas were initially hyperintense at both field strengths (Figs. 4F, 4I, 6E, and 6H). At 1.5 T, a thin iso- to hypointense rim was interposed between central and peripheral regions of hyperintensity, while at 0.6 T, uniform hyperintensity was seen. The subsequent appearance of central hypointensity was affected by both the field strength and the source of hemorrhage (Figs. 3C and 3D). Central hypointensity developed more rapidly and was more pronounced at 1.5 than at 0.6 T. In dog 6, for example, maximal hypointensity was reached as early as 12 hr at 1.5 T and at a minimum of 24 hr at 0.6 T (compare Figs. 4G and 4J); in dog 3, the degree of hypointensity was greater at 1.5 T (compare Figs. 5B and 5C). The source of hemorrhage affected hematoma intensity in that hypointensity evolved to its maximal extent by 12 hr in the two large venous hematomas compared with 60 hr in the large arterial hematoma (compare Figs. 4G and 6G). Variations in interecho interval (the time between 180° refocusing pulses) from 25 to 100 msec did not alter hematoma intensity when images with the same TE were compared.

As with the small hematomas, GE scans demonstrated hypointensity in all of the large hematomas regardless of the source of hemorrhage, the time from ictus, or the field strength (Figs. 4K, 4L, 6J, and 6K). Hypointensity was initially seen and was most pronounced at the margin of the hematoma, producing a ringlike appearance in many instances (Fig. 6J). Factors known to increase T2- or T2*-weighted contrast on GE images, such as decreasing the flip angle or increasing the TE, produced greater degrees of hypointensity, though these manipulations did not significantly enhance the ability to detect or delineate hemorrhage.

The two intraventricular hemorrhages (dogs 2 and 6), both produced with venous blood and both confirmed pathologically, behaved like the large arterial hematomas (Figs. 4 and 7). They demonstrated more rapid development of hyperintensity on short TR/TE images (Figs. 4D and 7A) and slower and less pronounced development of hypointensity on long TR/TE images (Figs. 4G and 7B) than did parenchymal clots of the same age. Because of the combined effects of hemorrhage location and field strength, the intraventricular hemorrhages did not develop hypointensity on long TR/TE scans at 0.6 T. On GE images, the intraventricular clots were markedly hypointense relative to CSF (and to gray matter) at both field strengths at all times and thus easily detectable (Figs. 4K and 4L).

The relative abilities of MR and CT to detect, delineate, and characterize hemorrhage were compared, with pathologic findings being used as the gold standard. MR was equal or superior to CT in detecting the presence of lesions. All of the hematomas produced intensity abnormalities on at least one pulse sequence at all times at both field strengths, while two of the small parenchymal hematomas and one of the intraven-

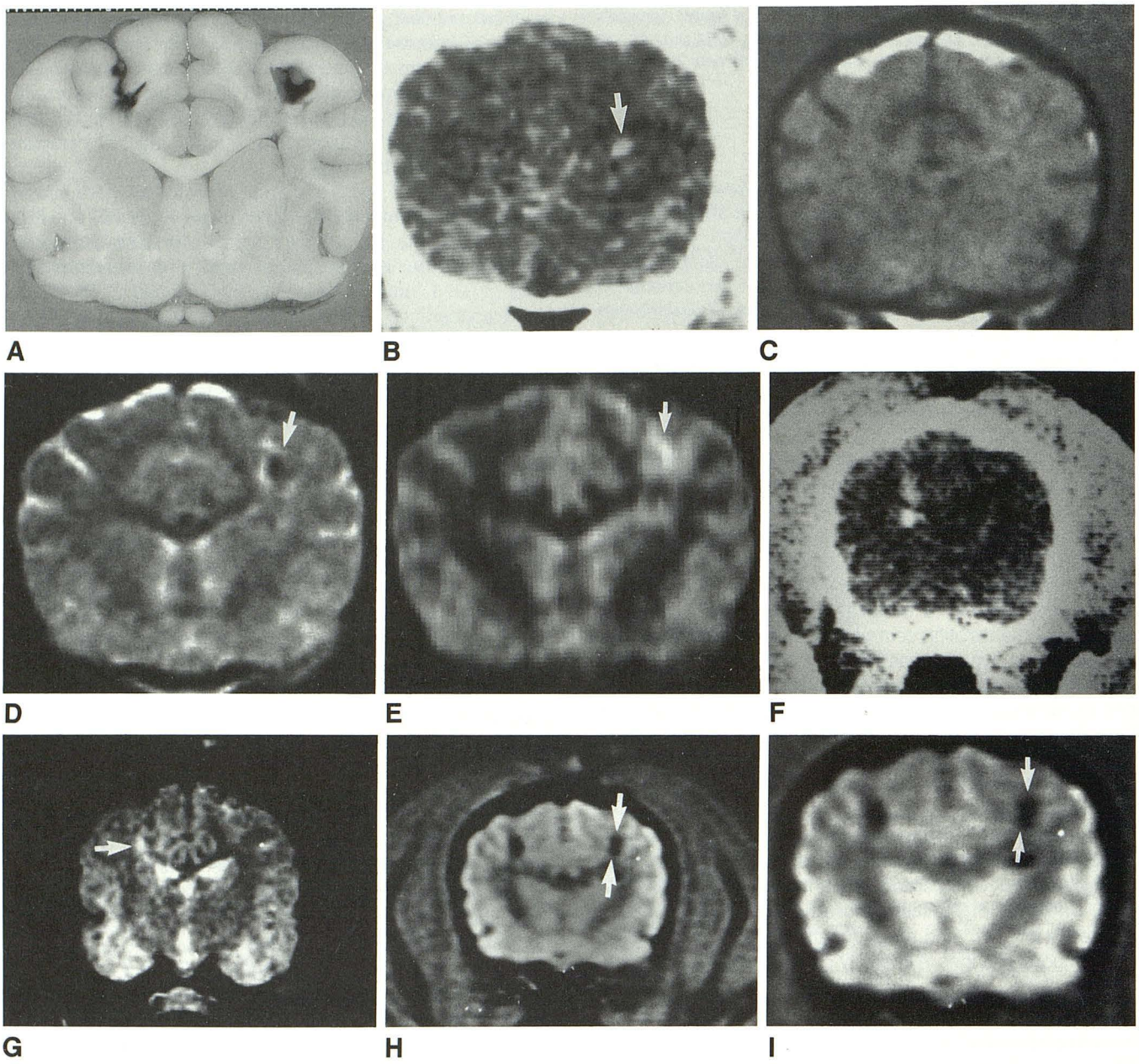

Fig. 2.—Dog 5: SE and GE imaging of two small arterial hematomas (A and B).
***A*, Pathologic specimen shows bifrontal hematomas.**
***B*, CT scan 4 hr after injection of hematoma A shows a left frontal hematoma (*arrow*).**
***C*, Short TR/TE image at 1.5 T 8 days after injection of hematoma A. Hematoma is not visible.**
***D*, Long TR/TE image at 1.5 T 0 hr after injection of hematoma A shows central hypointensity and peripheral hyperintensity (*arrow*).**
***E*, Long TR/TE image at 0.6 T 0 hr after injection of hematoma A shows homogeneous hyperintensity (*arrow*).**
***F*, CT scan 5 hr after injection of hematoma B shows a right frontal hematoma. Hematoma A, created 13 days earlier, is not seen.**
***G*, Long TR/TE image at 1.5 T immediately after injection of hematoma B shows a nonspecific intensity abnormality (*arrow*). Hematoma A is not seen.**
***H* and *I*, Corresponding GE images at 1.5 T (*H*) and 0.6 T (*I*) immediately after injection of hematoma B show hypointensity. Hypointensity persists in hematoma A (*arrows*), markedly improving its conspicuity compared with *F* and *G*.**

tricular hemorrhages were not seen on CT. In addition, the extent of hemorrhage was assessed more accurately with MR than with CT. Specifically, of the pulse sequences used, the GE sequences produced the most accurate delineation of all components of each hematoma when compared with gross pathology (compare Figs. 2H and 2I with 2A, 4K and 4L with 4A, and 6J and 6K with 6A). Moreover, GE scans were crucial in characterizing lesions as hemorrhagic, particularly before the development of hypointensity on long TR/TE scans and hyperintensity on short TR/TE scans.

The patient evaluated at 0.6 and 1.5 T sustained head trauma 60 hr before MR imaging. These studies, performed within 2 hr of each other (first at 0.6 T), demonstrated a subdural hematoma that was mildly hyperintense on short

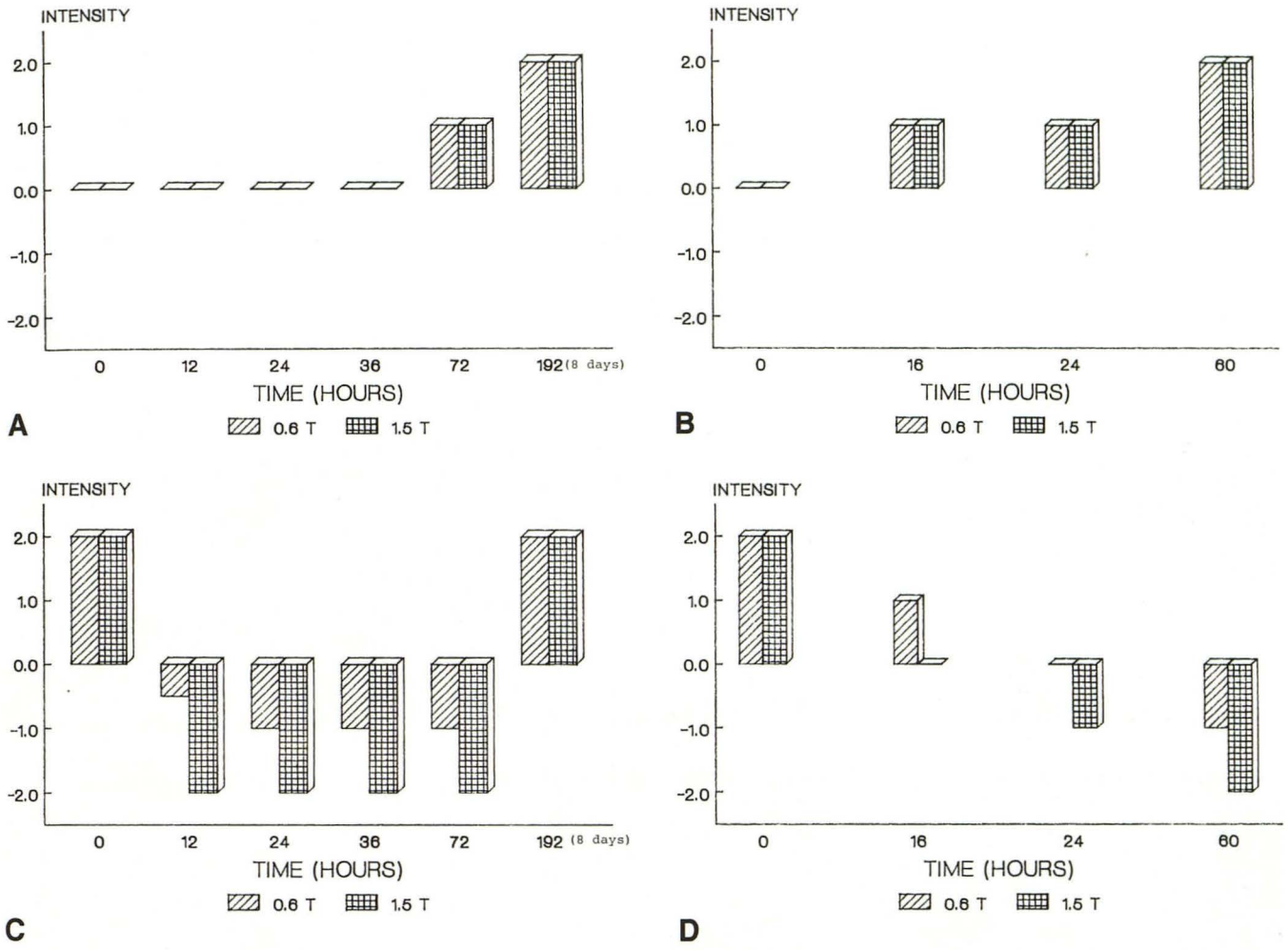

Fig. 3.—Time/intensity bar graphs for large hematomas.

***A* and *B*, Short TR/TE graphs for venous (*A*) and arterial (*B*) hematomas. Note that temporal changes and relative intensities are independent of field strength. Note also the development of hyperintensity at 72 hr in *A* vs 16 hr in *B*.**

***C* and *D*, Long TR/TE graphs for venous (*C*) and arterial (*D*) hematomas. Note initial hyperintensity at both field strengths in both sources of hemorrhage, more rapid development of hypointensity in venous hematomas, and more pronounced hypointensity at any given time at 1.5 T.**

TR/TE scans and hypointense on long TR/TE scans. There was no difference in the degree of hypointensity between the 0.6- and 1.5-T images (Fig. 8).

Discussion

This study was undertaken to improve our knowledge of the MR appearance of acute intracranial hemorrhage. Previous clinical studies [3, 6, 10] have documented that hematomas undergo complex changes in intensity during the first week. Initially, subtle hyperintensity on short TR/TE scans and hyperintensity on long TR/TE scans are seen. A thin hypointense rim may be visible at the margin of the hematoma on long TR/TE scans during this hyperacute stage. Within 48 hr, intensity decreases, resulting in iso- to mild hypointensity on short TR/TE scans and marked hypointensity on long TR/TE scans. On approximately the third to fifth postictal day, intensity increases, resulting in hyperintensity, usually peripheral in location, on short TR/TE scans. Subsequently, hyperintensity recurs on long TR/TE scans. Within this general framework, however, there are wide variations in the timing of these intensity changes, the extent to which they occur, and their location within each hematoma.

The cause or causes of these variations in hematoma intensity are difficult to evaluate with clinical studies since it is frequently impossible to precisely ascertain the interval between hemorrhage and MR imaging. In addition, critical factors including the source, size, and location of the hematoma and the presence of recurrent hemorrhage cannot be readily isolated, and hence, the individual contribution of each of these variables to hematoma intensity is difficult to assess.

The relationship between the magnetic field strength of the imager and the intensity of hemorrhage is another factor requiring further evaluation. Previous reports [3, 10] have stressed that, prior to the development of hyperintensity on short TR/TE scans, the presence of hypointensity on long TR/TE scans is the most critical factor in the detection of

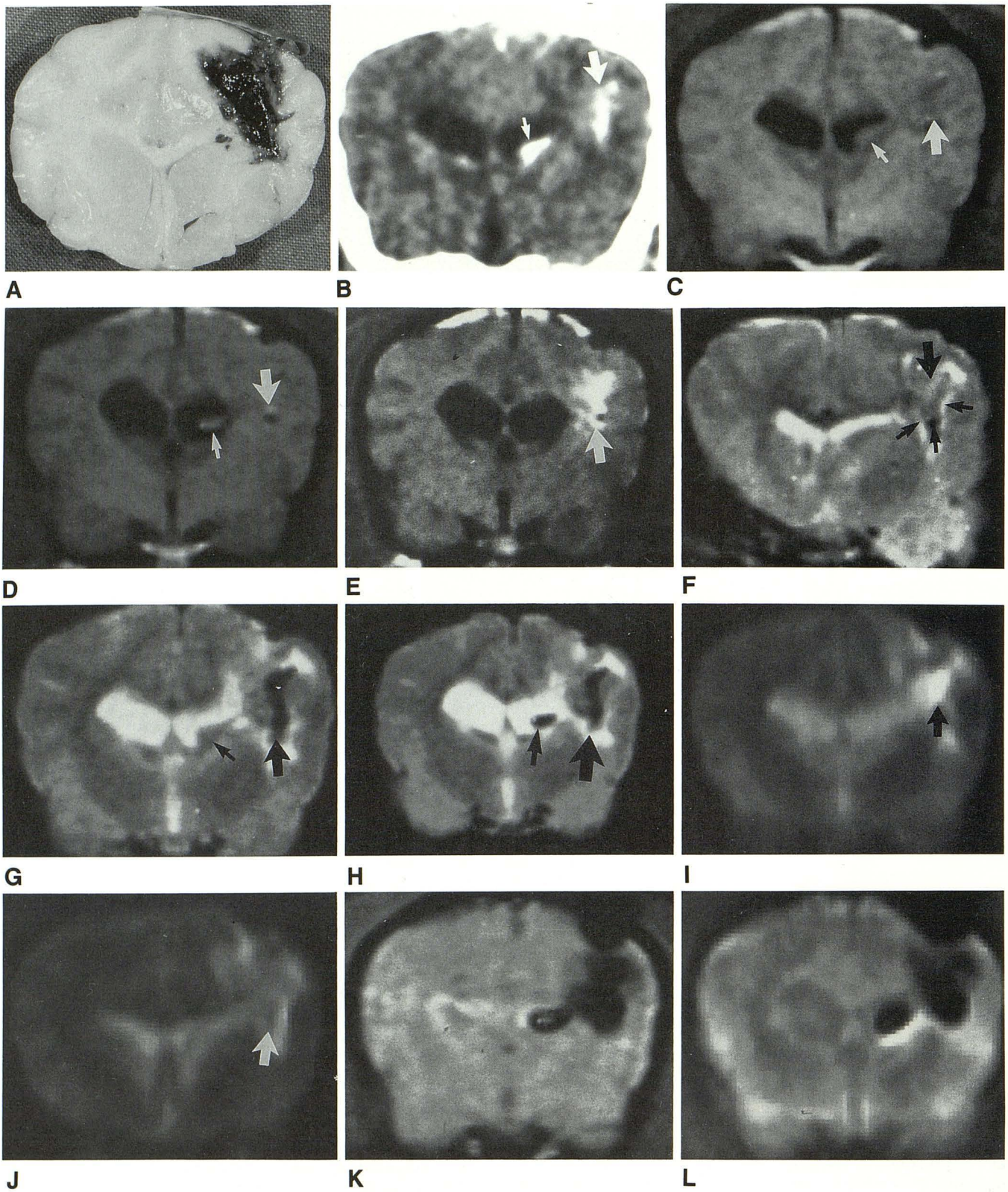
A
B
C
D
E
F
G
H
I
J
K
L

◀Fig. 4.—Dog 6: SE and GE imaging of a large venous hematoma with intraventricular extension.

A, Pathologic specimen shows parenchymal and intraventricular hemorrhages.

B, CT scan 4 hr after injection shows lateral portion of parenchymal hematoma (*large arrow*) and intraventricular hemorrhage (*small arrow*). Medial portion is less dense owing to partial-volume effect.

C–E, Short TR/TE images at 1.5 T at 0 hr (*C*), 72 hr (*D*), and 8 days (*E*) show initial isointensity of both parenchymal (*C*, *large arrow*) and intraventricular (*C*, *small arrow*) hemorrhages, initial appearance of parenchymal hyperintensity at 72 hr (*D*, *large arrow*), and progressive increase in hyperintensity by 8 days (*E*, *arrow*). Hyperintensity of intraventricular hematoma in *D* (*small arrow*) is greater than that of parenchymal hematoma.

F–H, Long TR/long TE images at 1.5 T at 0 (*F*), 12 (*G*), and 72 (*H*) hr show initial central (*F*, *large arrow*) and peripheral hyperintensity separated by a rim of mild hypointensity (*F*, *small arrows*), development of maximal hypointensity by 12 hr (*G*, *large arrow*), and no change at 24 hr (*H*, *large arrow*). Note slower development of hypointensity in intraventricular (*G* and *H*, *small arrows*) compared with parenchymal clot.

I and *J*, Long TR/TE images at 0.6 T at 0 (*I*) and 24 (*J*) hr show initial hyperintensity (*I*, *arrow*) followed by slower and less dramatic evolution of central hypointensity (*J*, *arrow*) compared with *G* and *H*. Intraventricular hemorrhage did not demonstrate hypointensity at any time on long TR/TE images at 0.6 T.

K and *L*, GE images at 72 hr at 1.5 T (*K*) and 0.6 T (*L*) show hypointensity in both parenchymal and intraventricular hemorrhages.

acute hemorrhage. Previous reports [3, 11, 12] also have indicated that the development of hypointensity is strongly related to the field strength of the MR imager.

An in vivo animal model seemed an ideal method for studying hemorrhage since the precise time from hemorrhage to MR imaging could be accurately determined; the source, size, and location of the hematoma could, in theory, be closely controlled; and serial studies could be readily performed as often as necessary during the early postictal period, where our knowledge of the appearance of acute hemorrhage is most limited.

All of the hematomas created were small (<2 cm in greatest dimension) compared with those typically encountered in clinical imaging, a result of the relatively small size of the dog's brain and the desire to avoid life-threatening mass effect from the injection of large amounts of blood. Therefore, the 1.5-T imager, with its thinner slices and smaller matrix size, was intrinsically superior to the 0.6-T unit in evaluating these small lesions irrespective of the presence of any field-strength–dependent factors affecting hematoma intensity. The size of the hematomas was, in fact, impossible to control precisely. The variability in hematoma size despite similar amounts of injected blood (Table 1), the result of dissection of blood along the injection tract or into the ventricular system, is a significant limitation of this animal model. However, the variability in hematoma size and location did have several unintentional benefits, including the detection of a clear-cut difference in behavior between small and large hematomas and the ability to directly compare parenchymal and intraventricular hemorrhages of the same age.

The lack of evolutionary changes in intensity in the four small hematomas was an unexpected finding. This static appearance may be related to the large surface area-to-volume ratio of the small hematomas, resulting in different physiochemical interactions with adjacent tissues, different rates of deoxyhemoglobin and methemoglobin formation, and different rates of clot formation and retraction. The findings in these small experimental hematomas mimic the "petechial" hemorrhages observed in patients with head trauma and hypertensive encephalopathy [13, 14], which, as in our model, are isointense and not detectable on short TR sequences, are of variable intensity and detectability on long TR images, and are always hypointense and readily detectable on GE scans. In addition, the lack of temporal changes in intensity may have implications for future animal models of hemorrhage, since data obtained from these obligatorily small hematomas may not be directly applicable to the larger hematomas generally seen in clinical practice.

The three large parenchymal and two intraventricular hematomas underwent serial intensity changes. However, there were considerable interhematoma variations mimicking (perhaps too well) the variations encountered in clinical imaging. This in turn made it difficult to define the precise effects of the various factors on hematoma intensity. Despite these limitations, several trends were identified.

On short TR/TE scans, hyperintensity developed 1–3 days

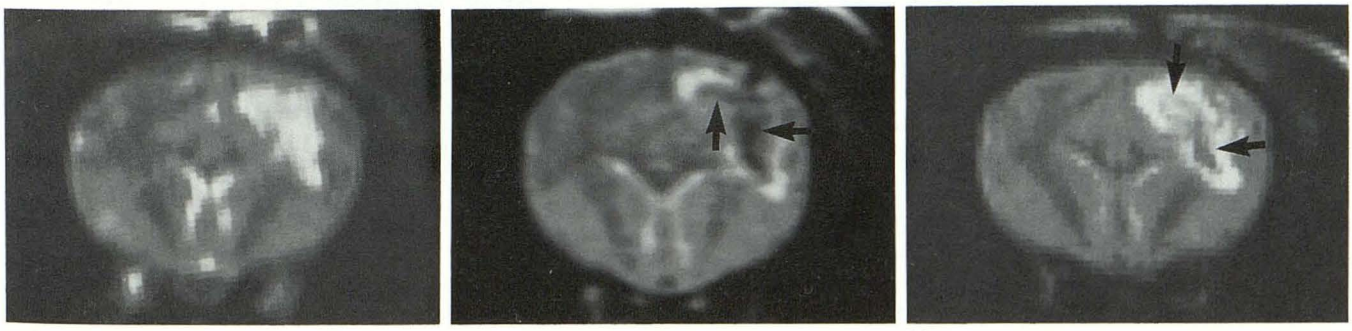

Fig. 5.—Dog 3: Effect of field strength on development of hypointensity in a large venous hematoma.

A, Long TR/TE image at 0.6 T at 0 hr shows homogeneous hyperintensity.

B and *C*, Long TR/TE images at 12 hr at 1.5 T (*B*) and 0.6 T (*C*) show development of central hypointensity at both field strengths (*arrows*), with more pronounced hypointensity at 1.5 T.

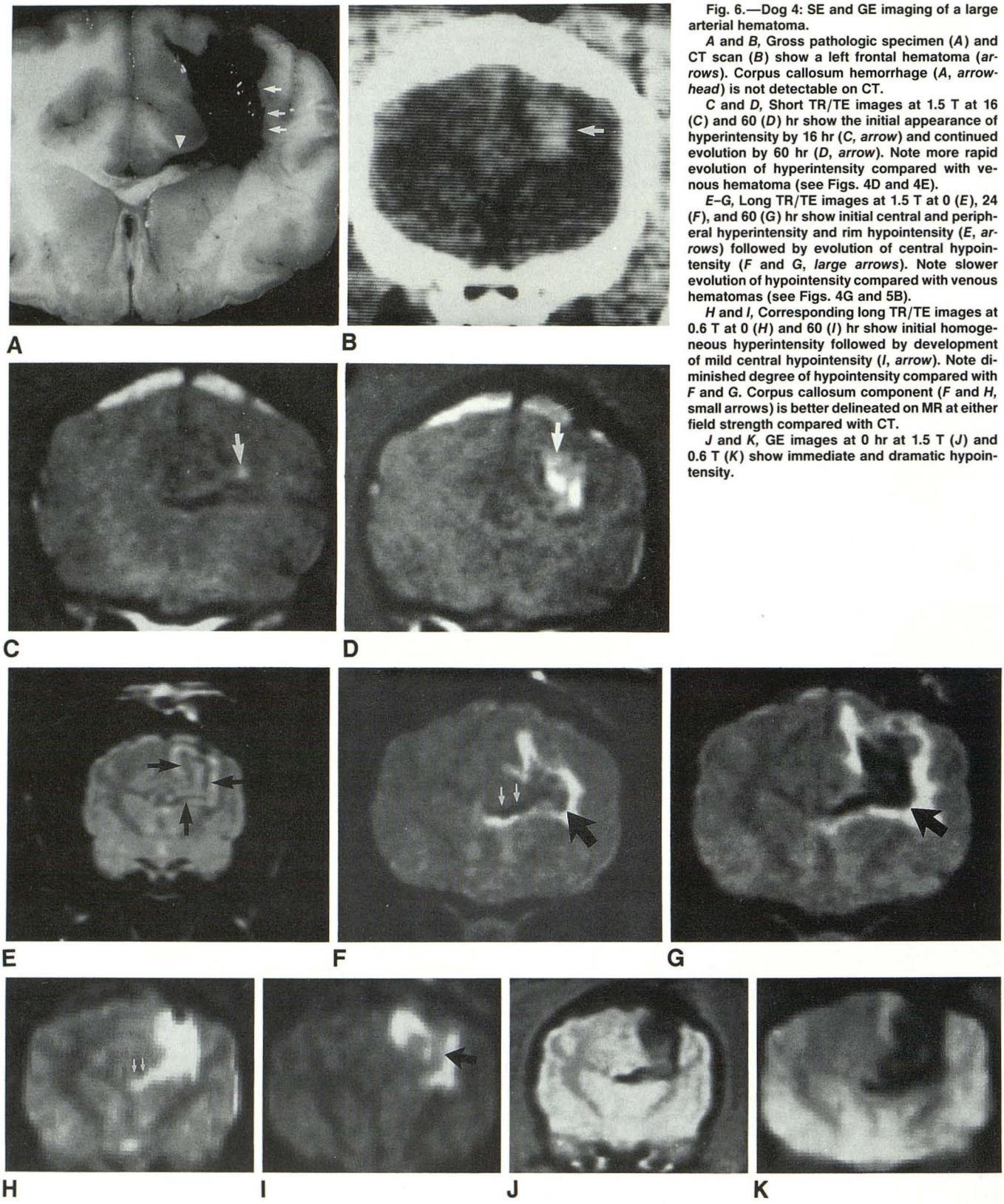

Fig. 6.—Dog 4: SE and GE imaging of a large arterial hematoma.

A and *B*, Gross pathologic specimen (*A*) and CT scan (*B*) show a left frontal hematoma (*arrows*). Corpus callosum hemorrhage (*A*, *arrowhead*) is not detectable on CT.

C and *D*, Short TR/TE images at 1.5 T at 16 (*C*) and 60 (*D*) hr show the initial appearance of hyperintensity by 16 hr (*C*, *arrow*) and continued evolution by 60 hr (*D*, *arrow*). Note more rapid evolution of hyperintensity compared with venous hematoma (see Figs. 4D and 4E).

E–G, Long TR/TE images at 1.5 T at 0 (*E*), 24 (*F*), and 60 (*G*) hr show initial central and peripheral hyperintensity and rim hypointensity (*E*, *arrows*) followed by evolution of central hypointensity (*F* and *G*, *large arrows*). Note slower evolution of hypointensity compared with venous hematomas (see Figs. 4G and 5B).

H and *I*, Corresponding long TR/TE images at 0.6 T at 0 (*H*) and 60 (*I*) hr show initial homogeneous hyperintensity followed by development of mild central hypointensity (*I*, *arrow*). Note diminished degree of hypointensity compared with *F* and *G*. Corpus callosum component (*F* and *H*, small arrows) is better delineated on MR at either field strength compared with CT.

J and *K*, GE images at 0 hr at 1.5 T (*J*) and 0.6 T (*K*) show immediate and dramatic hypointensity.

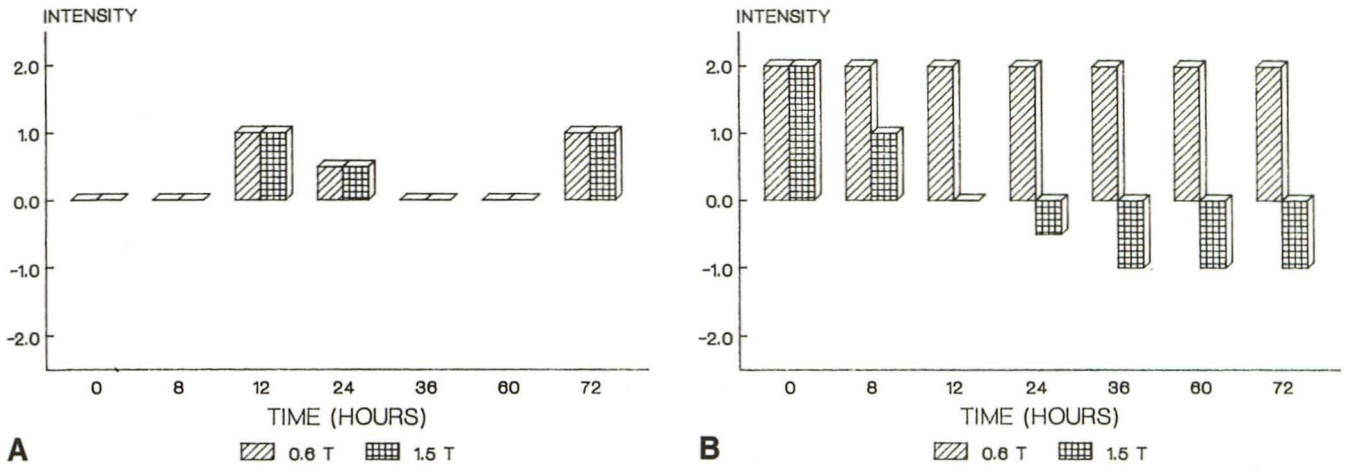

Fig. 7.—Time/intensity bar graphs of intraventricular hematomas, both of which were produced with venous blood.
***A*, Short TR/TE graph. Note more rapid development of hyperintensity compared with parenchymal hematomas (see Fig. 3A).**
***B*, Long TR/TE graph. Note lack of hypointensity at 0.6 T and slower development of hypointensity at 1.5 T compared with parenchymal hematomas (see Fig. 3C).**

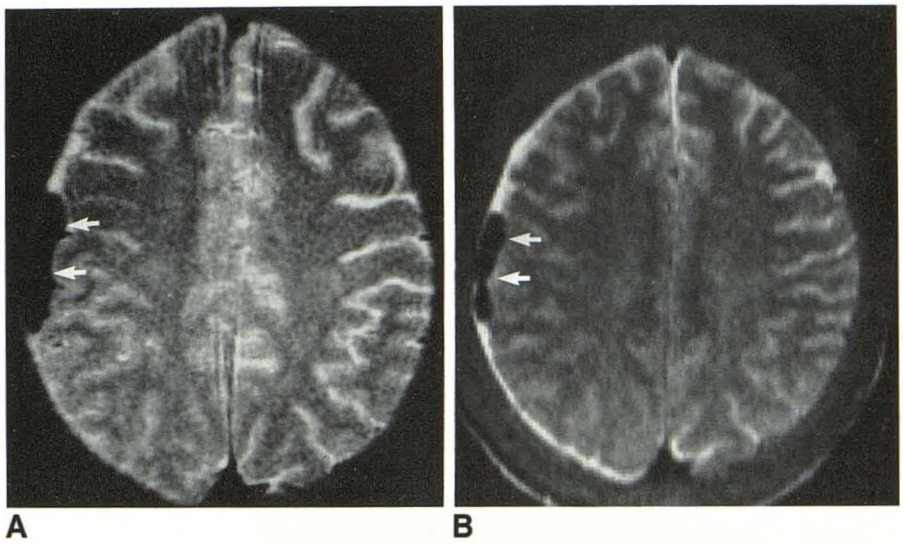

Fig. 8.—Effect of field strength on the development of hypointensity on long TR/TE scans in clinical imaging.
***A* and *B*, 1.5 T (*A*) and 0.6 T (*B*) images 60 hr after head trauma show no difference in degree of hypointensity in right convexity subdural hematoma (*arrows*).**

after hematoma generation. It occurred more rapidly in the arterial and intraventricular hematomas than in the venous clots. These findings were in accordance with previous clinical [3, 6, 15] and in vitro [15, 16] data. Hyperintensity is produced by methemoglobin, which causes paramagnetic T1 shortening due to proton-electron dipole-dipole interaction between water protons and the unpaired electrons of the methemoglobin molecule [3, 16]. Since the conversion of deoxyhemoglobin to methemoglobin is an oxidative process, it is not surprising that hyperintensity developed more rapidly in the arterial and intraventricular clots, which had a higher oxygen tension, than in the venous clots. We have observed a parallel situation in clinical imaging, where hemorrhage in the subarachnoid space may appear hyperintense within 36 hr on short TR/TE scans [17]. Field strength did not affect the rate or degree of development of hyperintensity on short TR/TE images. Previous studies had indicated that T1 shortening in hemorrhage may be more pronounced at lower field strengths (<0.15 T) [18], but this effect was not discernible within the range of field strengths evaluated in this experiment.

On long TR/TE scans there was a complex relationship between hematoma intensity and the time from ictus, field strength, hematoma source, and hematoma location. This study clearly documents the existence of a hyperacute phase during which hematomas are hyperintense relative to brain on long TR/TE scans at both 0.6 and 1.5 T. Subsequently, hypointensity developed more rapidly and to a greater degree at 1.5 than at 0.6 T. The finding of hyperintensity on MR images obtained at 1.5 T shortly after hemorrhage has not been documented clinically because currently few patients undergo MR imaging within the first few postictal hours. However, this finding has been reported on images obtained

at 0.6 T because the period of hyperintensity is longer at 0.6 T [6]. We anticipate that, as the use of MR in patients with acute neurologic dysfunction (<12 hr) increases, the hyperintense phase of hemorrhage will be seen with increasing frequency at all field strengths. Hence, knowledge of the existence of this phase of hemorrhage will be important for accurate diagnosis. Intuitively, one would also expect hypointensity to persist longer at high field strengths. In clinical practice, hypointensity at 0.6 T [6] begins to disappear on long TR/TE scans just after hyperintensity develops on short TR/TE sequences (3–4 days) and is typically resolved by 7 days, while hypointensity at 1.5 T [3, 10] has been noted to persist throughout the first week.

The field strength of the MR imager can be viewed as one factor affecting the rate of development and regression of hypointensity rather than the factor causing the presence or absence of this phenomenon. This hypothesis is supported by the limited number of clinical cases studied at both intermediate and high field strengths. In our patient evaluated at 60 hr, a sufficient amount of time for hypointensity to develop to a maximal degree at both 0.6 and 1.5 T, equal degrees of hypointensity were demonstrated. On the other hand, six of the seven acute hematomas studied by Seidenwurm et al. [10] were already hyperintense on short TR scans, and therefore were probably 4–7 days old. Hence, the greater degree of hypointensity detected in some of these hematomas at 1.5 T probably reflects prior resolution rather than failure of development of hypointensity.

The source and location of hemorrhage affected hematoma intensity. Arterial and intraventricular hemorrhage showed delayed development of hypointensity at 1.5 T and delayed and diminished development of hypointensity at 0.6 T. These findings shed light on the variability in hematoma intensity encountered in clinical imaging. Specifically, in patients with head injury imaged at 0.6 T, we have observed the slower development of hypointensity in epidural hematomas (arterial) than in parenchymal and subdural hematomas (venous or mixed) of the same age, while hypointensity may fail to develop in subarachnoid and intraventricular clots [17].

The mechanisms that have been proposed to explain the intensity of acute hematomas can be assessed in view of the findings from this study. The hyperintensity of hyperacute hematomas reflects the intensity of blood prior to the development of postextravasation biochemical and physiologic changes. Normal intraluminal blood is hypointense on long TR/TE scans owing to flow effects and turbulence, but becomes hyperintense, similar to hyperacute hematomas, when its signal is captured via even-echo rephasing, flow compensation, or cardiac gating [19]. This intensity is to be expected, given that blood is a proteinaceous fluid with a higher water content and therefore a longer T2 than brain parenchyma.

The subsequent development of hypointensity on long TR images has been attributed to the accumulation of paramagnetic deoxyhemoglobin within the relatively hypoxic hematoma center [3, 16]. When deoxyhemoglobin is intracellular, it causes local field inhomogeneities that produce rapid dephasing of water protons within and adjacent to these RBCs (susceptibility effect) [3, 20, 21]. Our findings are in general agreement with this hypothesis; however, the presence of hypointensity at 0.6 T in this study and in broad clinical experience supports the conclusion that the quadratic relationship between field strength and T2 proton relaxation enhancement in vitro [3, 12, 16] is not directly applicable in vivo. Recent in vitro studies [22–24] have demonstrated that hemoconcentration, clot formation, and retraction and diminution in RBC volume all may produce T2 shortening. These processes, with exception of hemoconcentration, are independent of the applied field strength [9]. Thus, we hypothesize that hypointensity in acute hematomas is the product of a number of contemporaneous but independent biochemical and physiologic phenomena, with the precise contribution of each factor dependent on the extent to which it is occurring in a given hematoma. This multifactorial hypothesis does not deny the significance of field-strength–dependent susceptibility effects. In fact, the importance of this mechanism of T2 shortening is preserved in the face of a much greater prevalence and degree of hypointensity in acute hematomas at intermediate and low field strengths than was initially predicted. At the same time, the marked variations in the timing and degree of hypointensity encountered in clinical imaging are accommodated.

This multifactorial hypothesis can be used to explain the differences in intensity between venous, arterial, and intraventricular hemorrhages. Arterial blood has a lower initial deoxyhemoglobin concentration (5%) than venous blood (40%), and therefore the development of hypointensity on long TR images is retarded at all field strengths and diminished (owing to decreased sensitivity to susceptibility effects) at intermediate field strength. Retardation and diminution in the development of hypointensity are more pronounced with intraventricular compared with parenchymal hemorrhage because of the effects of CSF on all of the causes of T2 shortening. Specifically, deoxyhemoglobin concentration is lower owing to the higher oxygen tension of spinal fluid, clot formation and retraction are inhibited, hemoconcentration is absent, and RBCs may swell rather than shrink [25]. The multifactorial hypothesis may also explain why prolongation of the interecho interval does not increase the degree of hypointensity on long TR scans in acute hemorrhage in vivo [26], as predicted from in vitro studies [11].

The findings from GE imaging of the three large and two intraventricular hemorrhages are the most dramatic and clinically significant results of this study. GE scans demonstrated readily detectable hypointensity regardless of the time from ictus, the source of location of hemorrhage, or the field strength. In addition, the GE scans were the most accurate of all of the MR pulse sequences, and more accurate than CT, in predicting the extent of hemorrhage on pathologic examination. The GE scans were most valuable in those circumstances in which intensity changes suggestive of hemorrhage, that is, hypointensity on long TR/TE scans and hyperintensity on short TR/TE scans, were absent. Thus, GE imaging had the greatest utility in hyperacute (<12 hr) hemorrhage at either field strength and in acute arterial and intraventricular hemorrhages at intermediate field strength. These experimental findings are in accordance with data from

previous clinical studies [27] and confirm the early prediction of Edelman et al. [28] on the efficacy of this technique in the evaluation of patients with hyperacute and acute hemorrhage. Nonetheless, GE imaging has limitations. Phase-shift artifacts induced by the bone/brain/air interface at the skull base make it difficult, if not impossible, to detect diffuse subarachnoid hemorrhage. Furthermore, hypointensity on GE scans is characteristic but not pathognomonic of hemorrhage, as it may be seen in other processes such as calcification [29].

Hypointensity on GE scans is the result of susceptibility effects induced by internal field inhomogeneities, to which GE pulse sequences are extremely sensitive [28]. Acute hematomas (1–7 days) are hypointense because they contain paramagnetic heterogeneously distributed (intracellular) deoxy- and methemoglobin. The source of hypointensity in hyperacute hematomas is less clear-cut, since at this stage minimal deoxyhemoglobin (5% in arterial blood and 40% in venous blood) and minimal or no methemoglobin are present. It is possible that GE scans are sensitive to even these small amounts of paramagnetic heme-proteins. Hayman et al. [30] have recently found that "macroscopic susceptibility effects" may occur as a result of irregular clumping of blood elements during early clot formation, resulting in hypointensity on GE imaging. Edelman et al. [28] noted that hypointensity on GE images was most pronounced near the periphery of the hematoma, a finding observed in our experimental hematomas, and suggested that this was due to a boundary effect between the hematoma and adjacent brain. This effect also may account for the hypointense rim seen in hyperacute hematomas on long TR/TE SE images in this study.

In conclusion, this study documents the effects of various parameters including the size of the hematoma, the source and location of hemorrhage, the time from ictus, and the field strength of the MR imager on hematoma intensity. On the basis of this study, it appears that GE sequences will prove highly useful in detecting and delineating all hemorrhages. Because of this, we strongly recommend that GE imaging be incorporated in the MR protocol for all patients with acute neurologic ictus or in whom hemorrhage is suspected.

REFERENCES

1. Sipponen JT, Sepponen RE, Sivula A. Nuclear magnetic resonance (NMR) imaging of intracerebral hemorrhage in the acute and resolving phases. *J Comput Assist Tomogr* **1983**;7:954–959
2. Bradley WG, Schmidt PG. Effect of methemoglobin formation on the MR appearance of subarachnoid hemorrhage. *Radiology* **1985**;156:99–103
3. Gomori JM, Grossman RI, Goldberg HI, Zimmerman RA, Bilaniuk LT. Intracranial hematomas: imaging by high-field MR. *Radiology* **1985**;157:87–93
4. Di Chiro GG, Brooks RA, Girton ME, et al. Sequential MR studies of intracerebral hematomas in monkeys. *AJNR* **1986**;7:193–199
5. Chakeres DW, Bryan RN. Acute subarachnoid hemorrhage: in vitro comparison of magnetic resonance and computed tomography. *AJNR* **1986**;7:223–228
6. Zimmerman RD, Heier LA, Snow RB, Liu DPC, Kelly AB, Deck MDF. Acute intracranial hemorrhage: intensity changes on sequential MR scans at 0.5 T. *AJNR* **1988**;9:47–57
7. Hayman LA, McArdle CB, Taber KH, et al. MR imaging of hyperacute intracranial hemorrhage in the cat. *AJNR* **1989**;10:681–686
8. Brooks RA, Di Chiro G, Patronas N. MR imaging of cerebral hematomas at different fields strengths: theory and applications. *J Comput Assist Tomogr* **1989**;13(2):194–206
9. Clark RA, Watanabe AT, Bradley WG, Roberts JD. Acute hematomas: effects of deoxygenation, hematocrit, and fibrin-clot formation and retraction T2 shortening. *Radiology* **1990**;175:201–206
10. Seidenwurm D, Meng T-K, Kowalski H, Weinreb JC, Kricheff II. Intracranial hemorrhagic lesions: evaluation with spin-echo and gradient-refocused MR imaging at 0.5 and 1.5T. *Radiology* **1989**;172:189–194
11. Gomori JM, Grossman RI, Yu-Ip C, Asakura T. NMR relaxation times of blood: dependence on field strength, oxidation state, and cell integrity. *J Comput Assist Tomogr* **1987**;11(4):684–690
12. Thulborn KR, Waterton JC, Matthews PM, Radda GK. Oxygenation dependence of the transverse relaxation time of water protons in whole blood at high field. *Biochim Biophys Acta* **1982**;714:265–270
13. Haimes AB, Zimmerman RD, Weingarten K, Kelly AB, Snow RD, Deck MDF. Role of gradient-echo imaging at 0.6T in the evaluation of head trauma. *Radiology* **1988**;169(P):309
14. Weingarten K, Zimmerman RD, Barbut D, Deck MDF. Malignant hypertension and hypertensive encephalopathy: MR imaging. *AJNR* **1989**;10:871
15. Gomori JM, Grossman RI, Hackney DB, Goldberg HI, Zimmerman RA, Bilaniuk LT. Variable appearances of subacute intracranial hematomas on high-field spin-echo MR. *AJNR* **1987**;8:1019–1026
16. Gomori JM, Grossman RI. Mechanisms responsible for the MR appearance and evolution of intracranial hemorrhage. *RadioGraphics* **1988**;8(3):427–440
17. Zimmerman RD. Magnetic resonance imaging of intracranial hemorrhage. In: Sarwar M, Batnitzky S, eds. *Nontraumatic ischemic and hemorrhagic disorders of the central nervous system.* Boston: Kluwer Academic Publishers, **1989**:1–55
18. Sipponen JT, Sepponen RE, Tanttu JI, Sivula A. Intracranial hematomas studied by MR imaging at 0.17 and 0.02T. *J Comput Assist Tomogr* **1985**;9(4):698–704
19. Bradley WG. Flow phenomena in MR imaging. *AJR* **1988**;150:983–994
20. DeLaPaz RL, New PFJ, Buonanno FS, et al. NMR imaging of intracranial hemorrhage. *J Comput Assist Tomogr* **1984**;8(4):599–607
21. Brooks RA, Brunetti A, Alger JR, Di Chiro G. On the origin of paramagnetic inhomogeneity effects in blood. *Magn Reson Med* **1989**;12:241–248
22. Hayman LA, Ford JJ, Taber KH, Saleem A, Round ME, Bryan RN. T2 effect of hemoglobin concentration: assessment with in vitro MR spectroscopy. *Radiology* **1988**;168:489–491
23. Hayman LA, Pagani JJ, Kirkpatrick JB, Hinck VC. Pathophysiology of acute intracerebral and subarachnoid hemorrhage: applications to MR imaging. *AJNR* **1989**;10:457–461
24. Hayman LA, Taber KH, Ford JJ, et al. Effect of clot formation and retraction on spin-echo MR images of blood: an in vitro study. *AJNR* **1989**;10:1155–1158
25. Jensen RS, Taber KH, Ford JJ, Plishker GA, Hayman LA. New factor in MR imaging of blood: water content of red blood cells. *Radiology* **1989**;173(P):221
26. Weingarten K, Zimmerman RD, Cahill PT, Deck MDF. Detection of acute intracerebral hemorrhage on MR imaging: ineffectiveness of prolonged interecho interval pulse sequences. *AJNR* **1991**;12:475–479
27. Weingarten K, Zimmerman RD, Haimes AB, Deck MDF. Acute cerebral infarction: evaluation with gradient-echo MR imaging. *Radiology* **1988**;169(P):310
28. Edelman RR, Johnson K, Buxton R, et al. MR of hemorrhage: a new approach. *AJNR* **1986**;7:751–756
29. Atlas SW, Mark AS, Grossman RI, Gomori JM. Intracranial hemorrhage: gradient-echo MR imaging at 1.5T. *Radiology* **1988**;168:803–807
30. Hayman LA, Ford JJ, Taber KH, Pagani JJ, Kirkpatrick JB. Importance of clot formation in gradient-echo imaging of blood. *AJNR* **1989**;10:895